Superhydrophobic, carbon-infiltrated carbon nanotubes on Si and 316L stainless steel with tunable geometry

Cite as: Appl. Phys. Lett. **112**, 211602 (2018); https://doi.org/10.1063/1.5034471 Submitted: 11 April 2018 . Accepted: 09 May 2018 . Published Online: 22 May 2018

Kimberly A. Stevens, Christian D. Esplin , Taylor M. Davis, D. Jacob Butterfield, Philip S. Ng, Anton E. Bowden, Brian D. Jensen, and Brian D. Iverson







ARTICLES YOU MAY BE INTERESTED IN

Micro-architecture embedding ultra-thin interlayer to bond diamond and silicon via direct fusion

Applied Physics Letters 112, 211601 (2018); https://doi.org/10.1063/1.5030580

Controlling the surface photovoltage on WSe₂ by surface chemical modification Applied Physics Letters 112, 211603 (2018); https://doi.org/10.1063/1.5026351

Roll-to-roll fabrication of hierarchical superhydrophobic surfaces
Applied Physics Letters 113, 041601 (2018); https://doi.org/10.1063/1.5037946







Superhydrophobic, carbon-infiltrated carbon nanotubes on Si and 316L stainless steel with tunable geometry

Kimberly A. Stevens, Christian D. Esplin, Taylor M. Davis, D. Jacob Butterfield, Philip S. Ng, Anton E. Bowden, Brian D. Jensen, and Brian D. Iverson^{a)}

Mechanical Engineering Department, Brigham Young University, Provo, Utah 84604, USA

(Received 11 April 2018; accepted 9 May 2018; published online 22 May 2018)

The use of carbon nanotubes to create superhydrophobic coatings has been considered due to their ability to offer a relatively uniform nanostructure. However, carbon nanotubes (CNTs) may be considered delicate with a typical diameter of tens of nanometers for a multi-walled CNT; asgrown carbon nanotubes often require the addition of a thin-film hydrophobic coating to render them superhydrophobic. Furthermore, fine control over the diameter of the as-grown CNTs or the overall nanostructure is difficult. This work demonstrates the utility of using carbon infiltration to layer amorphous carbon on multi-walled nanotubes to improve structural integrity and achieve superhydrophobic behavior with tunable geometry. These carbon-infiltrated carbon nanotube (CICNT) surfaces exhibit an increased number of contact points between neighboring tubes, resulting in a composite structure with improved mechanical stability. Additionally, the native surface can be rendered superhydrophobic with a vacuum pyrolysis treatment, with contact angles as high as 160° and contact angle hysteresis on the order of 1°. The CICNT diameter, static contact angle, sliding angle, and contact angle hysteresis were examined for varying levels of carbon-infiltration to determine the effect of infiltration on superhydrophobicity. The same superhydrophobic behavior and tunable geometry were also observed with CICNTs grown directly on stainless steel without an additional catalyst layer. The ability to tune the geometry while maintaining superhydrophobic behavior offers significant potential in condensation heat transfer, anti-icing, microfluidics, antimicrobial surfaces, and other bio-applications where control over the nanostructure is beneficial. Published by AIP Publishing. https://doi.org/10.1063/1.5034471

Since their discovery, the unique properties of carbon nanotubes (CNTs) have made them a popular option for creating superhydrophobic surfaces. In particular, CNTs offer the ability to create a relatively uniform nanostructure, facile options for altering the surface chemistry (i.e. hydrophobic coatings or modification to the native surface chemistry), and flexibility in the configuration (e.g. ability to grow directly onto a substrate, create patterns at the microscale, create two-tiered surfaces, etc.). Such properties have allowed superhydrophobic CNTs to be used in a range of applications such as enhanced droplet mobility during condensation, ^{1–5} oil-water filtration, ^{6,7} absorption, ⁸ self-cleaning, drag reduction, ⁹ antifouling, ¹⁰ lab-on-chip, creation of antimicrobial surfaces, ^{11–13} and other bio-applications.

Carbon-infiltrated carbon nanotubes (CICNTs), also known as densified carbon nanotubes or carbon nanotube/carbon composite fibers, ^{14–21} are composed of CNTs with additional layers of carbon deposited on the nanotube framework. The resulting composite is stronger than CNTs alone ^{14–19} and can display higher electrical conductivity, ¹⁴ depending on the level of infiltration.

Superhydrophobic surfaces are considered to have a solid/liquid contact angle greater than 145° and low contact angle hysteresis. ^{22,23} Commonly, superhydrophobic surfaces are created through a combination of tailored surface roughness and surface chemistry. As described above, CNTs have been used to provide nanoscale surface roughness. Since

as-grown CNTs are frequently not hydrophobic, CNT surfaces have been rendered superhydrophobic through the addition of a non-wetting coating using silanes, fluorination, or polymers like poly(tetrafluoroethylene) (PTFE). 1-5,24-27

However, post-growth surface treatments have also been shown to alter the wettability of carbon surfaces. Various plasma treatments have been used to render as-grown CNTs superhydrophobic. ^{20,28} Li *et al.* demonstrated that the hydrophobicity of native CNTs could be controlled using reactive ion etching and laser pruning. ²⁹ Others have demonstrated that CNT surfaces can be changed from a superhydrophobic state to a superhydrophilic state using UV and ozone treatment. ^{30–33} These groups have also shown that the process can be reversed to render non-infiltrated CNT surfaces superhydrophobic by heating CNTs in a vacuum (i.e. vacuum pyrolysis). ^{30–33}

This work demonstrates that CICNTs can also be rendered superhydrophobic using vacuum pyrolysis, eliminating the need for deposition of a non-wetting coating. We also quantify the surface wetting characteristics for patterned and unpatterned, two-tiered superhydrophobic CICNT surfaces. Further, we demonstrate that similar superhydrophobic CICNT surfaces can be grown directly on 316L stainless steel without the need for a catalyst. Finally, we explore the influence of the degree of carbon infiltration on the CICNT diameter, static contact angle, sliding angle, and contact angle hysteresis.

CICNT surfaces were grown in three different microscale patterns on alumina-coated silicon wafers. CNTs were grown to achieve (1) a blanket forest of CNTs uniformly

^{a)}Author to whom correspondence should be addressed: bdiverson@byu.edu

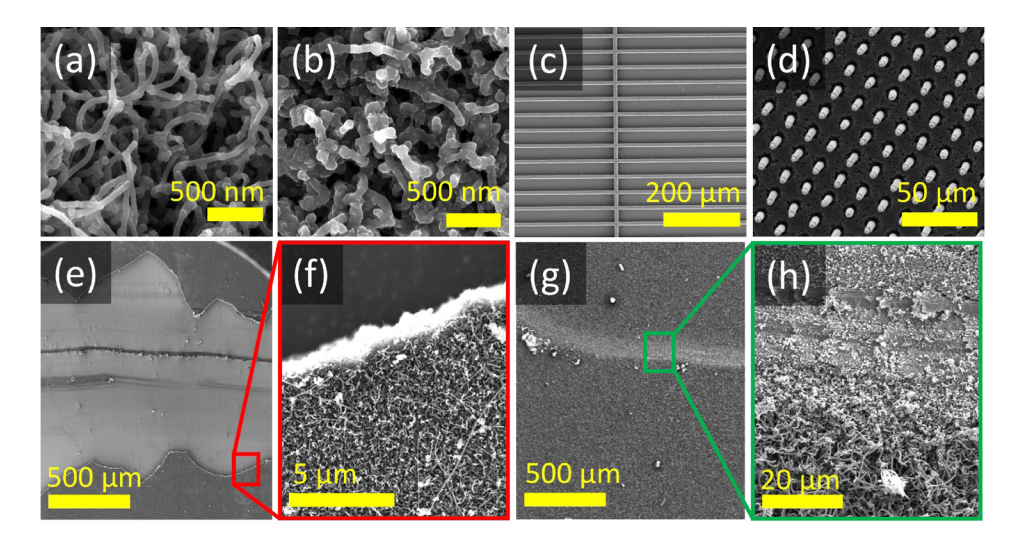


FIG. 1. (a) Top-down view of vertically aligned CNT forest without infiltration. (b) Top-down view of a CICNT forest with reduced porosity and inter-CNT spacing. Microscale (c) rib and (d) post pattern composed of CICNTs. (e)—(h) SEM images showing where a diamond scribe scratched CICNTs grown on (e) and (f) Si with an Fe catalyst and on (g) and (h) 316L stainless steel without a catalyst (direct growth). CICNTs remain attached to the stainless steel surfaces everywhere except where they came in direct contact with the diamond scribe.

coating the surface [Figs. 1(a) and 2(b)]; (2) a microscale rib pattern [Fig. 1(c)]; and (3) an array of cylindrical posts [Fig. 1(d)]. The rib width and spacing in Fig. 1(c) are 8 μ m and $40 \,\mu\text{m}$, respectively, resulting in 20% surface coverage by CICNT structures. The post diameter and pitch in Fig. 1(d) are 7 μ m and 16 μ m, respectively, resulting in 15% surface coverage by CICNT structures in a square arrangement. Standard photolithographic and lift-off procedures were used to pattern a 7 nm layer of Fe as a catalyst for CNT growth. Diced, Fe-patterned samples were placed in a Lindberg/Blue M tube furnace for CNT growth by flowing H2 gas (373.6 sccm) and C_2H_4 gas (204.0 sccm) at $750 \,^{\circ}\text{C}$ for 15 s. After growth, the multi-walled CNTs achieved a height of approximately 20 µm. The CNTs were then coated (infiltrated) with amorphous carbon in the furnace by flowing H₂ (444.88 sccm) and C_2H_4 (204.0 sccm) at $900 \,^{\circ}\text{C}$ for 0, 5, 10, or 15 min. Above 15 min, delamination of the porous carbon structure was observed from the Si substrate, likely due to

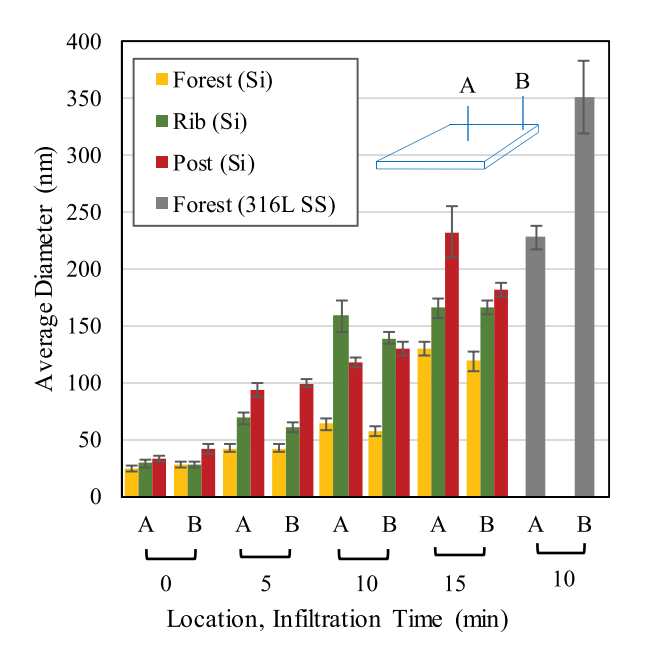


FIG. 2. Average diameter of the CICNTs for different infiltration times. Each measurement is the average of at least 20 carbon nanotubes with error bars representing the 95% confidence interval. Measurements were taken at locations (a) near the center and (b) near the corner of square samples.

internal stresses in the film. Infiltration times may vary for different furnace setups but with similar decreasing porosity with increasing infiltration time.

CICNTs were also grown directly on the as-received 316L stainless steel substrates with a #8 mirror finish without an additional catalyst layer (hereafter referred to as direct growth), as opposed to indirect growth with CICNTs grown on stacked layers of Fe and alumina on Si. Samples were placed in a Lindberg/Blue M tube furnace and air annealed by ramping to 800 °C while flowing Ar gas and then held for 2 min while flowing air. CNT growth was achieved by flowing Ar (311.0 sccm) and C₂H₄ (338.0 sccm) at 800 °C for 20 min. The CNTs were then infiltrated with amorphous carbon in the furnace by flowing Ar (311.0 sccm) and C₂H₄ (338.0 sccm) at 900 °C for 10 min. The direct growth CICNTs were grown in a blanket forest with no microscale pattern.

Once the CICNTs were grown and infiltrated, the surfaces were vacuum annealed (i.e. vacuum pyrolysis) at approximately 17 kPa and 250 °C for 24 h to remove the absorbed oxygen and achieve superhydrophobic behavior. ³³ Prior to vacuum pyrolysis, the forest patterned surfaces displayed static contact angles of approximately 90°, as described by others. ^{24,27}

The diameter of the infiltrated nanotubes was measured from top-down imaging using scanning electron microscopy, similar to those shown in Figs. 1(a) and 1(b). Variation in the diameter of the coated nanotubes was observed and may be attributed to (1) natural variation in the size due to variations in the catalyst, (2) variation in the diameter along the height of the nanotube, and (3) variable proximity of neighboring nanotubes. For this reason, a minimum of 20 measurements for diameter were averaged for characterization and the 95% confidence interval was reported.

Contact angle measurements were obtained using the sessile drop method. An approximately 2 mm water drop was deposited on test surfaces, backlit with illumination from an LED light, and imaged with a high-resolution camera. A fifth-order polynomial fit was obtained for the droplet profile near the triple point contact line. The tangent line at the intersection of the polynomial fit and contact line was reported as the contact angle, with an accuracy of $+/-2^{\circ}$. Contact angles from left and right sides were then averaged

together. Advancing and receding contact angles were obtained by quasi-statically expanding and contracting the drop by adding and subtracting liquid volume with a needle while recording the drop with a video camera. 36,37 The advancing and receding contact angles were evaluated by post-processing video images in a similar manner to the static contact angle. The difference between the advancing and receding contact angles is the contact angle hysteresis. The sliding angle, or the angle at which a stationary, 2 mm drop began to slide away from its original location, was measured using a micrometer angle gauge, accurate to within $+/-0.5^{\circ}$.

The mean diameter of CICNTs for varying infiltration times is shown in Fig. 2. For each infiltration time and pattern, measurements were taken at two locations on square samples: one near the center of the sample (location A) and the other near the corner (location B), as shown in the figure. As expected, more amorphous carbon was deposited during the longer infiltration times, leading to larger average diameters. The spatial location for the diameter measurement of the CICNTs grown on Si had no significant effect on the average diameter. Samples that were infiltrated for 15 min had average nanotube diameters more than 400% larger than those with no infiltration for all surface patterns. The ability to tune the diameter of the structures by varying the infiltration time offers an additional element of surface feature control to CNT growth.

The microscale pattern influenced the rate of deposition of amorphous carbon and thus the average diameter of the structures. The forest pattern consistently exhibited the smallest diameters of the patterns tested for all infiltration times. CICNTs grown in the rib pattern generally had smaller diameters than those grown in the post pattern. This trend of increased infiltration may be due to the availability of more carbon atoms in the C₂H₄ gas or reduced obstruction of the gas for lower density microscale patterning. Jeong *et al.* observed a similar trend, where less-dense patterns grew taller CNT structures compared to their scaled, moredense counterparts.³⁸

Diameters of CICNTs grown directly on stainless steel were significantly larger than the indirect growths; however, the size of the CICNTs as a function of infiltration time may not be directly compared between direct and indirect growth samples since the furnace conditions and substrates were different. The large variation in the diameter size with spatial location reflects a general trend of large variation in diameter size for direct growth CICNTs.

Following vacuum pyrolysis treatment, all surfaces exhibited superhydrophobic behavior. The average static contact angle for each of the surfaces is shown in Fig. 3, with values greater than 145°. The superhydrophobicity was stable, with insignificant changes in the contact angle over time. Each measurement is the average of measurements taken at 3–4 different locations on the surface; the variation is represented by the error bars, which are one standard deviation above and below the average. The contact angle did not change significantly with the CICNT diameter, microscale pattern type, or substrate. Though the average contact angle is slightly lower for the surfaces with CNTs grown in a post pattern, the larger variation (reflected in the standard deviation) in static contact angle and larger contact angle

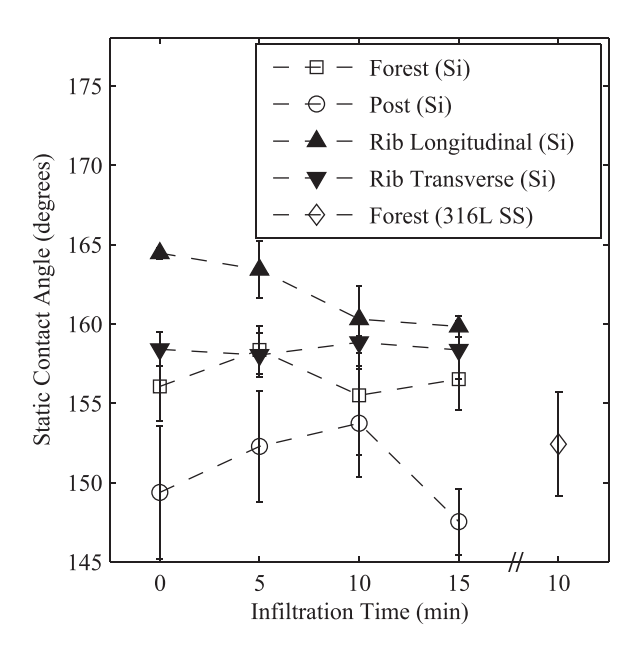


FIG. 3. Static contact angle of water droplets on CICNT surfaces. Each measurement is the average contact angle taken at 3 or 4 different locations. The error bars are ± 1 1 standard deviation. The contact angle does not vary significantly with the CICNT diameter, infiltration time, substrate, or microscale pattern.

hysteresis could be indicative of a larger number of defects on the surface. Indeed, the surfaces with CNTs grown in a post pattern were observably less robust than the other surfaces. Considering the extremely high aspect ratio of the carbon nanotubes (height $\sim\!20~\mu{\rm m}$ and diameter 25–200 nm), it is not surprising that when the carbon nanotubes were grown in small islands, they were not observed to be as strong since the network of interconnected CNTs was smaller. Regardless of the infiltration time or microscale pattern, the average static contact angle for all surfaces resulted in superhydrophobic behavior.

In addition to having high static contact angles, each of the surfaces exhibited extremely low contact angle hysteresis, on the order of 1°. Each measurement in Table I is the average of hysteresis measurements taken at four different locations on the surface. Rib-patterned surfaces with four measurements included two measurements in each direction. All variations in contact angle hysteresis are within the measurement uncertainty, regardless of surface pattern or infiltration time. The sliding angle, another indicator of droplet mobility, was measured on surfaces of each pattern type and across a range of infiltration times. As expected from the low hysteresis, small sliding angle values of less than 1°-3° were observed, with no significant variation with the infiltration time or pattern. All of the surfaces exhibited static contact angle and droplet mobility measurements that qualify them as superhydrophobic, and the degree of superhydrophobicity appeared to be largely independent of infiltration time or pattern over the range tested.

The foregoing results demonstrate that carbon infiltration can be used to tune the diameter of the carbon nanotubes and that following a vacuum pyrolysis treatment, the carbon infiltrated carbon nanotubes are superhydrophobic, without the need for an additional hydrophobic coating. Even significant changes in the microscale arrangement, structure size,

TABLE I. Average of 2–4 hysteresis measurements on sample surfaces. The sliding angle was always less than 1° – 3° regardless of surface geometry, infiltration time, and location. Neither hysteresis nor sliding angle varies significantly with the microscale pattern, CICNT diameter, infiltration time, or substrate.

Pattern	Infiltration time (min)	Hysteresis (degrees)	Sliding angle (degrees)
Forest (Si)	0	0.3	<1-3
	10	0.2	
	15	0.9	
Post (Si)	0	0.8	
	10	2.4	
Rib longitudinal (Si)	0	< 0.1	
	15	0.7	
Rib transverse (Si)	0	0.5	
	15	1.8	
Forest (316L SS)	10	1.7	

and substrate type (direct vs indirect) did not appear to influence the hydrophobicity of the resulting surface. CICNTs were also observed to be oleophilic; a drop of machine oil placed on the surface had a static contact angle of 35°.

The direct growth CICNTs on 316L stainless steel were observably more robust than the indirect growth surfaces on Si. To demonstrate their robustness, a diamond scribe was used to scratch a direct and indirect growth surface. SEM images of the scratches are shown in Figs. 1(e)–1(h). On the indirect growth surface, a large section of the CICNT film delaminated and detached. However, on the direct growth surface, the scribe scratched the stainless steel surface, but CICNTs remain attached everywhere except where they came in direct contact with the diamond scribe. Direct growth CICNTs appeared to be less vertically aligned than the indirect growth sample on Si; the increase in random growth direction potentially resulted in an increase in the level of CNT interconnectedness, thus improving structural integrity.

The ability to tune nanoscale geometry without affecting hydrophobicity creates new possible applications for superhydrophobic CNTs. For example, superhydrophobic surfaces have shown great potential in the area of condensation heat transfer, where the droplet growth, coalescence, and departure are dependent on the nanostructure and feature sizes. 1.2,39,40 Mulroe *et al.* showed that the greater the nanoscale roughness (i.e. more tall, slender nanostructures as opposed to short, stout structures), the smaller the departure size of the drops, a parameter that is directly related to the rate of thermal transport. The ability to tune the nanoscale geometry of superhydrophobic surfaces used in condensation is a desirable trait with carbon infiltration affording the possibility to control CNT geometry.

Carbon nanotubes can be enhanced by infiltrating with amorphous carbon to improve mechanical durability, ¹⁴ increase resistance to shear failure, ^{14–19} and control the nanoscale feature size. CICNT structures can be rendered superhydrophobic for a range of infiltration rates with negligible change in superhydrophobicity, as determined by the static contact angle, contact angle hysteresis, and sliding angle. In general, longer infiltration times result in carbon

nanotubes with larger diameters, and the rate of infiltration is somewhat dependent on the patterning of carbon nanotubes, with sparser microscale patterning leading to higher rates of infiltration. Superhydrophobicity is invariant to the infiltration rate/CICNT diameter within the range tested here. CICNTs grown directly on stainless steel surfaces, when subjected to vacuum pyrolysis, display the same superhydrophobic properties as those on Fe deposited on alumina. Surfaces created with direct growth of CICNTs on the stainless steel are even more robust than CICNTs grown on Fe deposited on alumina, as partially demonstrated by the scratch tests presented in this work. The ability to grow CICNTs directly on the stainless steel without the need for Fe deposition reduces fabrication complexity and increases potential scalability of these surfaces.

¹H. Cha, J. M. Chun, J. Sotelo, and N. Miljkovic, ACS Nano **10**(9), 8223–8232 (2016).

²H. Cha, C. Y. Xu, J. Sotelo, J. M. Chun, Y. Yokoyama, R. Enright, and N. Miljkovic, Phys. Rev. Fluids 1(6), 064102 (2016).

³C. H. Chen, Q. J. Cai, C. L. Tsai, C. L. Chen, G. Y. Xiong, Y. Yu, and Z. F. Ren, Appl. Phys. Lett. **90**(17), 173108 (2007).

⁴J. T. Cheng, A. Vandadi, and C. L. Chen, Appl. Phys. Lett. **101**(13), 131909 (2012).

⁵R. Enright, N. Miljkovic, J. Sprittles, K. Nolan, R. Mitchell, and E. N. Wang, ACS Nano 8(10), 10352–10362 (2014).

⁶C. H. Lee, N. Johnson, J. Drelich, and Y. K. Yap, Carbon **49**(2), 669–676 (2011)

⁷T. C. Huang, P. Li, H. Q. Yao, H. J. Sue, M. Kotaki, and M. H. Tsai, RSC Adv. 6(15), 12431–12434 (2016).

⁸X. Gui, J. Wei, K. Wang, A. Cao, H. Zhu, Y. Jia, Q. Shu, and D. Wu, Adv. Mater. 22(5), 617–621 (2010).

⁹B. Bhushan and Y. C. Jung, Prog. Mater. Sci. **56**(1), 1–108 (2011).

¹⁰M. Nosonovsky and B. Bhushan, Curr. Opin. Colloid Interface Sci. 14(4), 270–280 (2009).

¹¹S. Kang, M. Herzberg, D. F. Rodrigues, and M. Elimelech, Langmuir 24(13), 6409–6413 (2008).

¹²A. Al-Jumaili, S. Alancherry, K. Bazaka, and V. M. Jacob, Materials 10(9), 1066 (2017).

¹³L. M. Hoyos-Palacio, A. G. García, J. F. Pérez-Robles, J. González, and H. V. Martínez-Tejada, IOP Conf. Ser.: Mater. Sci. Eng. 59(1), 012005 (2014).

¹⁴X. S. Li, L. Ci, S. Kar, C. Soldano, S. J. Kilpatrick, and P. M. Ajayan, Carbon 45(4), 847–851 (2007).

¹⁵J. Lee, T. Kim, Y. Jung, K. Jung, J. Park, D. M. Lee, H. S. Jeong, J. Y. Hwang, C. R. Park, K. H. Lee, and S. M. Kim, Nanoscale 8(45), 18972–18979 (2016).

¹⁶Q. M. Gong, Z. Li, D. Li, X. D. Bai, and J. Liang, Solid State Commun. 131(6), 399–404 (2004).

¹⁷Q. M. Gong, Z. Li, X. D. Bai, D. Li, Y. Zhao, and J. Liang, Mater. Sci. Eng. 384(1-2), 209–214 (2004).

¹⁸B. H. Hanna, W. C. Fazio, J. D. Tanner, J. M. Lund, T. S. Wood, R. C. Davis, R. R. Vanfleet, and B. D. Jensen, J. Microelectromech. Syst. 23(6), 1330–1339 (2014).

¹⁹K. Jones, B. D. Jensen, and A. Bowden, J. Nanotechnol. Eng. Med. 4(2), 020903–020907 (2013).

²⁰Z. J. Han, B. K. Tay, M. Shakerzadeh, and K. Ostrikov, Appl. Phys. Lett. 94(22), 223106 (2009).

²¹Z. Han, B. Tay, C. Tan, M. Shakerzadeh, and K. Ostrikov, ACS Nano 3(10), 3031–3036 (2009).

²²K.-Y. Law, J. Phys. Chem. Lett. **5**(4), 686–688 (2014).

²³W. Chen, A. Y. Fadeev, M. C. Hsieh, D. Oner, J. Youngblood, and T. J. McCarthy, Langmuir 15(10), 3395–3399 (1999).

²⁴K. K. S. Lau, J. Bico, K. B. K. Teo, M. Chhowalla, G. A. J. Amaratunga, W. I. Milne, G. H. McKinley, and K. K. Gleason, Nano Lett. 3(12), 1701–1705 (2003).

²⁵H. J. Li, X. B. Wang, Y. L. Song, Y. Q. Liu, Q. S. Li, L. Jiang, and D. B. Zhu, Angew. Chem. Int. Ed. 40(9), 1743–1746 (2001).

²⁶S. Li, H. Li, X. Wang, Y. Song, Y. Liu, L. Jiang, and D. Zhu, J. Phys. Chem. B **106**(36), 9274–9276 (2002).

²⁷H. Liu, J. Zhai, and L. Jiang, Soft Matter **2**(10), 811–821 (2006).

- ²⁸Y. C. Hong and H. S. Uhm, Appl. Phys. Lett. **88**(24), 244101 (2006).
- ²⁹P. H. Li, X. D. Lim, Y. W. Zhu, T. Yu, C. K. Ong, Z. X. Shen, A. T. S. Wee, and C. H. Sow, J. Phys. Chem. B 111(7), 1672–1678 (2007).
- ³⁰H. Z. Wang, Z. P. Huang, Q. J. Cai, K. Kulkarni, C. L. Chen, D. Carnahan, and Z. F. Ren, Carbon 48(3), 868–875 (2010).
- ³¹A. Aria and M. Gharib, in *Nanotech 2011: Technical Proceedings of the 2011 NSTI Nanotechnology Conference and Expo* (2011), Vol. 1, pp. 149–152.
- ³²A. I. Aria and M. Gharib, Langmuir **27**(14), 9005–9011 (2011).
- ³³A. I. Aria and M. Gharib, J. Visualized Exp.: JoVE (74), 50378 (2013).
- ³⁴E. Atefi, J. A. Mann, and H. Tavana, Langmuir **29**(19), 5677–5688 (2013).
- ³⁵A. Bateni, S. S. Susnar, A. Amirfazli, and A. W. Neumann, Colloids Surf. A: Physicochem. Eng. Aspects 219(1), 215–231 (2003).
- ³⁶L. Gao and T. J. McCarthy, Langmuir **22**(14), 6234–6237 (2006).
- ³⁷J. Berg, *Wettability* (CRC Press, 1993).
- ³⁸G.-H. Jeong, N. Olofsson, L. K. L. Falk, and E. E. B. Campbell, Carbon 47(3), 696–704 (2009).
- ³⁹M. D. Mulroe, B. R. Srijanto, S. F. Ahmadi, C. P. Collier, and J. B. Boreyko, ACS Nano 11(8), 8499–8510 (2017).
- ⁴⁰R. Enright, N. Miljkovic, A. Al-Obeidi, C. V. Thompson, and E. N. Wang, Langmuir **28**(40), 14424–14432 (2012).